

# A method for simulating level anti-crossing spectra of diamond crystals containing NV<sup>-</sup> color centers

S.V. Anishchik<sup>1,\*</sup> and K.L. Ivanov<sup>2,3,†</sup>

<sup>1</sup>*Voevodsky Institute of Chemical Kinetics and Combustion SB RAS, 630090, Novosibirsk, Russia*

<sup>2</sup>*International Tomography Center SB RAS, 630090, Novosibirsk, Russia*

<sup>3</sup>*Novosibirsk State University, 630090, Novosibirsk, Russia*

We propose an efficient method for calculating level anti-crossing spectra (LAC spectra) of interacting paramagnetic defect centers in crystals. By LAC spectra we mean the magnetic field dependence of the photoluminescence intensity of paramagnetic color centers: such field dependences often exhibit sharp features, such as peaks or dips, originating from LACs in the spin system. Our approach takes into account the electronic Zeeman interaction with the external magnetic field, dipole-dipole interaction of paramagnetic centers, hyperfine coupling of paramagnetic defects to magnetic nuclei and zero-field splitting. By using this method, we can not only obtain the positions of lines in LAC spectra, but also reproduce their shapes as well as the relative amplitudes of different lines. As a striking example, we present a calculation of LAC spectra in diamond crystals containing negatively charged NV centers.

PACS numbers: 61.72.jn, 75.30.Hx, 78.55.-m, 81.05.ug

## I. INTRODUCTION

Owing to their unique properties [1] negatively charged nitrogen-vacancy centers, NV<sup>-</sup> centers, in diamond crystals are promising quantum objects for various exciting applications, such as, e.g., nano-sensing [2–6], quantum information processing [7–11], imaging of biological processes [12–15]. Experiments with NV<sup>-</sup> centers exploit optically detected magnetic resonance, allowing one to probe the spin dynamics of single color centers [16, 17], i.e., of single quantum objects. Such extraordinary sensitivity, along with extremely long spin memory times and decoherence times [18] make feasible various challenging experiments. Importantly, such properties are preserved even at room temperature [19–21], which dramatically extends the range of existing and potential applications of NV<sup>-</sup> centers. One of the key issues for such applications is interaction of NV<sup>-</sup> centers with other defect centers of the diamond lattice. Since such defect centers are often “dark” centers, information about such interactions can be deduced indirectly from Level Anti-Crossing (LAC) spectra. Experimentally such LAC spectra of diamond single crystals containing NV<sup>-</sup> centers can be studied by monitoring the magnetic field dependence of the photoluminescence intensity, which contains sharp features associated with LACs [21–35]. To probe such “LAC lines” no resonant microwave or radiofrequency pumping is required.

The scheme of the energy levels of an NV<sup>-</sup> center at zero external magnetic field is shown in Fig. 1, with radiative and radiationless optical transitions and radiofrequency-driven spin transitions indicated. The ground state of the defect center is an electronic triplet

state. Due to zero-field splitting (ZFS) in the absence of a field the lowest state in energy is the state with zero projection, denoted as  $M_s$ , of the electron spin on the NV<sup>-</sup> center symmetry axis, hereafter denoted as  $\mathbf{r}_{NV}$ . The excited state has a similar structure of the spin energy levels, but with a smaller ZFS value (by approximately a factor of two). For practical applications of NV<sup>-</sup> centers, it is important that the “optical cycle” gives rise to strong spin polarization [36–39]. The mechanism of polarization formation is given by the dependence of the inter-system crossing rates on the spin projection value  $M_s$ .

Due to the peculiarities of the optical cycle, there is a strong difference in the luminescence quantum yield upon excitation of an NV<sup>-</sup> in the spin states with different  $M_s$  values. When excitation occurs from the  $M_s = 0$  state, the yield of subsequent photoluminescence is close to unity. For this reason, the  $M_s = 0$  state is a “bright” state of the color center. By contrast, after excitation from the  $M_s = \pm 1$  states the luminescence yield is small due to the fast intersystem crossing process  $^3E \rightarrow ^1A_1$ ; hence, these states are “dark” states. Owing to the fact that the  $^1E \rightarrow ^3A_2$  process is also dependent on the  $M_s$  value (it is fast for the  $M_s = 0$  state); after light irradiation the system goes to the  $M_s = 0$  state. This means that the ground state of the NV<sup>-</sup> center acquires spin polarization [36, 40, 41]. Hence, NV<sup>-</sup> centers can be spin-polarized by light excitation; such spin-polarized states can also be studied by optically detected magnetic resonance by using the remarkable property that NV<sup>-</sup> centers have “bright” and “dark” spin states.

Spin dynamics of NV<sup>-</sup> centers can be thus probed via photoluminescence, which also strongly depends on the magnetic field. The reason is that at specific field strengths mixing of the “bright” and “dark” states takes place, which gives rise to a drop in the luminescence intensity. Specifically, such mixing becomes efficient at LACs, which give rise to sharp features in the field de-

\* svan@kinetics.nsc.ru

† ivanov@tomo.nsc.ru

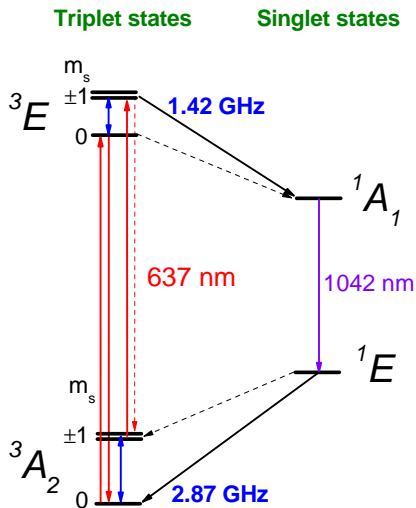


FIG. 1. Energy levels of an  $\text{NV}^-$  center at zero magnetic field. By arrows we show the zero-phonon line optical transitions, inter-system crossing between the triplet and singlet states and RF-induced transitions in the ground and excited states. Strong transitions are shown by solid lines, weak transitions are shown by dashed lines. States of the  $\text{NV}^-$  center are classified according to the spin multiplicity and irreducible representations,  $A$  and  $E$ , of the  $C_{3v}$  point group. ZFS of each triplet state is indicated, as well as the wavelengths of the optical transitions.

pendence of luminescence.

As usual, by a LAC we mean the following situation. Let us assume that at a field strength  $B_0 = B_{LC}$  a level crossing occurs for a pair of levels,  $E_\mu$  and  $E_\nu$ , corresponding to the eigen-states  $|\mu\rangle$  and  $|\nu\rangle$  of the main part of the spin Hamiltonian  $\hat{H}_0$ . However, if there is also a perturbation term to the full Hamiltonian, i.e.,  $\hat{H} = \hat{H}_0 + \hat{V}$ , such that  $V_{\mu\nu} = \langle\mu|\hat{V}|\nu\rangle \neq 0$ , the levels never cross. In the mathematical sense this means that the  $\mu$ -th and  $\nu$ -th eigen-states of  $\hat{H}$  are different at any field; the minimal splitting between them at  $B_0 = B_{LC}$  is equal to  $2|V_{\mu\nu}| \neq 0$ . In other words, the crossing is avoided: the level crossing turns into a LAC. Importantly, at the LAC not only the degeneracy of the energy levels is lifted, but also the eigen-states change: the true eigen-states are no longer given by  $|\mu\rangle$  and  $|\nu\rangle$  but by superposition states. As a result, mixing of the  $|\mu\rangle$  and  $|\nu\rangle$  states takes place. For this reason, LACs are of importance for analyzing the magnetic field dependence of the photoluminescence intensity of  $\text{NV}^-$  centers: at a LAC involving a “bright” state and a “dark” state the intensity drops because initially over-populated “bright” state becomes mixed with the “dark” state. Dips in the magnetic field dependence of the photoluminescence intensity are thus associated with such LACs. Therefore, we hereafter term this field dependence “LAC spectrum”.

Simulation of LAC spectra remains a challenging problem because of the need to model the spin dynamics in a complex multi-level system. As we show below, for

simulating some LAC lines one should treat a multi-spin system, which dramatically increases the dimensionality of the spin Hamiltonian matrices. In principle, full quantum mechanical treatment of polarization transfer, which would explicitly include the dynamics in both triplet states,  $^3A$  and  $^3E$ , is possible [28, 34, 42, 43]; however, it requires introducing the density matrix of a multi-level system (including the energy levels of the excited states) and working in the Liouville space rather than in the Hilbert space. As a consequence, the dimensionality of the Liouville super-matrices becomes too large and numerical solution of the equation for the density matrix of the system becomes extremely time consuming, if at all possible. In the present case, this problem is further aggravated by the necessity to take into account a second defect center, to which polarization is transferred from the primarily polarized  $\text{NV}^-$  center. For this reason, we use simplifying assumptions, which allow us to treat redistribution of the light-induced spin polarization in a system of two coupled defect centers having magnetic nuclei. The simulation method proposed here is numerically efficient and relatively easy to implement. As we show below, this approach allows one to model LAC spectra, being able to reproduce not only the positions of LAC lines (including weak satellites to main lines) but also their relative amplitudes. Hence, we are able to simulate LAC spectra, model LAC lines and assign them to interaction of specific pairs of interacting defect centers. This work is thus important for developing methods for detection of “dark” defect centers in diamond crystals.

## II. EXPERIMENTAL

The experimental method is described in detail in a previous publications [28, 34]. All experiments were carried out using single crystals of a synthetic diamond. The average concentration of  $\text{NV}^-$  centers was  $9.3 \times 10^{17} \text{ cm}^{-3}$ . The samples were placed in a magnetic field, which is a superposition of the constant field,  $\mathbf{B}_0$ , and a weak field modulated with the amplitude  $B_m$  at the frequency  $f_m$ , and irradiated by the laser light at a wavelength of 532 nm (the irradiation power was 400 mW). The beam direction was perpendicular to the magnetic field vector  $\mathbf{B}_0$ . The laser light was linearly polarized and the electric field vector  $\mathbf{E}$  was perpendicular to  $\mathbf{B}_0$ . In experiments, we precisely oriented the sample such that the magnetic field was parallel to the  $[111]$  crystal axis.

The luminescence intensity was measured by a photomultiplier. The resulting signal was sent to the input of a lock-in detector to increase the detection sensitivity. Such a method indeed allows one to enhance the sensitivity and to resolve multiple LAC lines. Due to lock-in detection, lines in experimental LAC spectra have dispersive shapes. For this reason, we also integrate the obtained LAC spectra and compare them to calculated spectra. The modulation frequency  $f_m$  was 17 Hz and modulation amplitude was  $B_m = 0.5 \text{ G}$ . All experiments

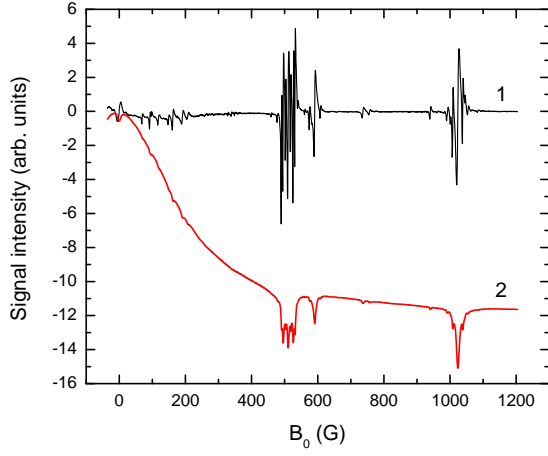


FIG. 2. Experimental LAC spectrum of a diamond single crystal containing  $\text{NV}^-$  centers. Here we show the signal obtained by using lock-in detection (curve 1) with the polarization of light  $\mathbf{E} \perp \mathbf{B}_0$  and the integrated spectrum (curve 2). The modulation frequency is 17 Hz, the modulation amplitude is 0.5 G.

were carried out at room temperature.

In this work, we present the experimental results, namely, LAC spectra, obtained earlier [34]. In Fig. 2 we present the LAC spectrum of the sample obtained by using lock-in detection of photoluminescence and also the integrated spectrum. Both spectra contain multiple sharp LAC lines. Below, we compare parts of the integrated spectrum with calculation results. We discuss only some of the LAC lines and do not model the lines, which are not yet assigned (these are the lines found in the range 50-250 G and lines at about 750 G and 950 G).

### III. THEORY

#### A. Spin Hamiltonian

Generally, the spin Hamiltonian  $\hat{H}$  of two interacting paramagnetic centers in the external  $\mathbf{B}_0$  field can be written as a sum of the main Hamiltonian and a perturbation term:

$$\hat{H} = \hat{H}_0 + \hat{V} \quad (1)$$

where

$$\hat{H}_0 = \beta \mathbf{B}_0 \mathcal{G}_1 \hat{\mathbf{S}}_1 + \hat{\mathbf{S}}_1 \mathcal{D}_1 \hat{\mathbf{S}}_1 + \beta \mathbf{B}_0 \mathcal{G}_2 \hat{\mathbf{S}}_2 + \hat{\mathbf{S}}_2 \mathcal{D}_2 \hat{\mathbf{S}}_2 \quad (2)$$

and

$$\begin{aligned} \hat{V} = & \sum_i \hat{\mathbf{S}}_1 \mathcal{A}_i \hat{\mathbf{I}}_i + \sum_i \hat{\mathbf{I}}_i \mathcal{Q}_i \hat{\mathbf{I}}_i + \sum_j \hat{\mathbf{S}}_2 \mathcal{A}_j \hat{\mathbf{I}}_j + \sum_j \hat{\mathbf{I}}_j \mathcal{Q}_j \hat{\mathbf{I}}_j \\ & + D_{dd} \left[ 3(\hat{\mathbf{S}}_1 \cdot \mathbf{n}_{12})(\hat{\mathbf{S}}_2 \cdot \mathbf{n}_{12}) - (\hat{\mathbf{S}}_1 \cdot \hat{\mathbf{S}}_2) \right], \quad (3) \end{aligned}$$

Here  $\hat{\mathbf{S}}_1$  and  $\hat{\mathbf{I}}_i$  are the electron and nuclear spin operators of the  $\text{NV}^-$  center,  $\hat{\mathbf{S}}_2$  and  $\hat{\mathbf{I}}_j$  correspond to the other

defect center. The main part of the Hamiltonian takes into account the electronic Zeeman interaction (described by the  $g$ -tensors  $\mathcal{G}_1$  and  $\mathcal{G}_2$  with  $\beta$  being the Bohr magneton) and ZFS (given by the ZFS tensors  $\mathcal{D}_1$  and  $\mathcal{D}_2$ ). The perturbation term includes the hyperfine couplings (HFCs) to magnetic nuclei (given by the HFC tensors  $\mathcal{A}_i$  and  $\mathcal{A}_j$ ), nuclear quadrupolar couplings (given by the tensors  $\mathcal{Q}_i$  and  $\mathcal{Q}_j$ ) and the electronic dipole-dipole interaction between the two centers, which depends on the distance between them:  $D_{dd} \propto r_{12}^{-3}$ , where  $\mathbf{r}_{12}$  is the vector connecting the two defect centers,  $\mathbf{n}_{12} = \mathbf{r}_{12}/r_{12}$  is unity length vector parallel to  $\mathbf{r}_{12}$ . Here, for simplicity, nuclear Zeeman interaction is neglected as we are working at relatively low magnetic fields. In this work, we will specify the Hamiltonian and all relevant parameters (HFC and quadrupolar couplings, ZFS values,  $D_{dd}$ ) in the units of Hz. In this work, all tensors are denoted by calligraphic capital letters.

The interaction terms in eqs. (2) and (3) come from anisotropic interactions and therefore depend on the molecular orientation and on the choice of the coordinate frame. The individual terms of the Hamiltonian become simple, when when the reference frame coincides with the Principal Axes System (PAS) of the corresponding interaction tensor: in such a frame the tensor simply becomes diagonal and its non-zero elements are the principle values of the tensor. As a consequence, the relevant terms in their PASs are written as follows (here  $k = 1, 2$ ):

$$\begin{aligned} \beta \mathbf{B}_0 \mathcal{G}_k \hat{\mathbf{S}}_k = & \beta \left[ g_{k,||} B_{0,z} \hat{S}_{kz} + g_{k,\perp} B_{0,x} \hat{S}_{kx} \right. \\ & \left. + g_{k,\perp} B_{0,y} \hat{S}_{ky} \right] \quad (4) \end{aligned}$$

$$\hat{\mathbf{S}}_k \mathcal{D}_k \hat{\mathbf{S}}_k = D_k \left[ \hat{S}_{kz}^2 - \frac{2}{3} \right] \quad (5)$$

$$\hat{\mathbf{S}}_k \mathcal{A}_i \hat{\mathbf{I}}_i = A_{i,||} \hat{S}_{kz} \hat{I}_{iz} + A_{i,\perp} \hat{S}_{kx} \hat{I}_{ix} + A_{i,\perp} \hat{S}_{ky} \hat{I}_{iy} \quad (6)$$

$$\hat{\mathbf{I}}_i \mathcal{Q}_i \hat{\mathbf{I}}_i = Q_i \left[ \hat{I}_{iz}^2 - \frac{1}{3} I_i(I_i + 1) \right]. \quad (7)$$

Here we take into account that all defect centers considered here have axial symmetry; consequently, the  $x, y$ -components of all tensors are identical (denoted by  $\perp$  instead of  $x, y$ ), generally, being different from the  $z$ -component (denoted by  $||$ ). Hence,  $g_{i,||}, g_{i,\perp}$  are the relevant components of the  $\mathcal{G}_k$  tensor;  $D_k$  is the relevant component of the ZFS tensor (hereafter we always assume that  $E_k = 0$ , i.e., due to axial symmetry the  $x$  and  $y$  directions are equivalent);  $A_{i,||}, A_{i,\perp}$  are the components of the  $\mathcal{A}_i$  tensor;  $Q_i$  is the quadrupolar coupling of the corresponding nucleus. In any frame different from PAS additional terms appear in the interaction tensor and, consequently, in the Hamiltonian. To define frame rotations one can use different methods, e.g., one can specify the three angles for consecutive Euler rotations. Here we

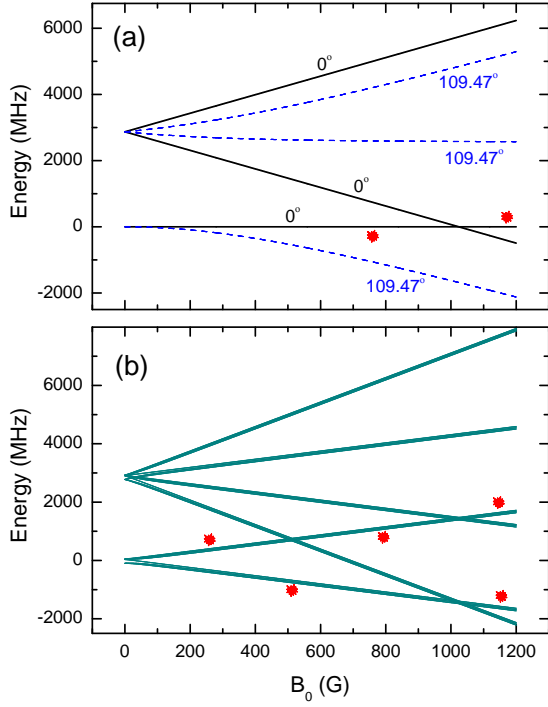


FIG. 3. Calculated energy levels of the ground state of an isolated  $\text{NV}^-$  center (a) and the system of  $\text{NV}^-$  and P1 centers (b) in an external magnetic field  $B_0$ . Stars highlight the “bright” energy levels of the  $\text{NV}^-$  center.

do not dwell into details of frame rotations, which are done in a standard way [44].

In this work, we always choose the reference frame such that the  $z$ -axis is parallel to the  $\mathbf{r}_{\text{NV}}$  vector of the first defect center (which is always an  $\text{NV}^-$  center). This means that the tensors  $\mathcal{G}_1$ ,  $\mathcal{D}_1$ ,  $\mathcal{A}_i$ ,  $\mathcal{Q}_i$  have the simple form given by eqs. (4)-(7). In this situation, if the  $\mathbf{B}_0$  vector is parallel to the [111] crystal axis, the magnetic field can be either parallel to  $\mathbf{r}_{\text{NV}}$ , so that only the  $B_{0,z}$  component is non-zero, or tilted by  $\theta_t = 109.47^\circ$  (tetrahedral angle), so that the transverse field components are present as well. For the second center we assume that it (i) has the same orientation meaning that the relevant interaction tensors also take the simple form, expected for the PAS or (ii) its orientation is tilted by  $\theta_t$  with respect to  $\mathbf{r}_{\text{NV}}$ .

In Fig. 3(a) we present the energy levels of a single isolated  $\text{NV}^-$  center for the two possible orientations with respect to the external magnetic field, which are existing when the [111] crystal axis is parallel to the  $\mathbf{B}_0$  field. Specifically, there is an orientation where  $\mathbf{r}_{\text{NV}}$  is parallel to  $\mathbf{B}_0$  (1/4 of all centers have this orientation) and an orientation where the angle between  $\mathbf{r}_{\text{NV}}$  and  $\mathbf{B}_0$  is equal to  $\theta_t$  (3/4 of all centers have this orientation). In Fig. 3 we show the energy levels for both possible orientations; in the calculation we take into account the Zeeman interaction, ZFS, HFC of the electron spin of the  $\text{NV}^-$  center with the spin of the nitrogen nucleus and nuclear quadrupolar coupling. When the angle between  $\mathbf{r}_{\text{NV}}$  and

$\mathbf{B}_0$  is equal to  $\theta_t$  there are no level crossings in the ground state. However, once  $\mathbf{r}_{\text{NV}}$  is parallel to  $\mathbf{B}_0$ , at the field of  $B_0 = D = 1024$  G there is a crossing between the “bright”  $M_s = 0$  level and the “dark”  $M_s = -1$  level. HFC turns this crossing into a LAC; spin mixing at this LAC brings the system from the  $M_s = 0$  state to the  $M_s = -1$  state. Consequently, the population of the “bright” state decreases, giving rise to a reduction of the photoluminescence intensity at this field. As a result, a sharp LAC line appears in the field dependence of the luminescence intensity, see Fig. 2.

In Fig. 3(b) as a representative example we present the calculated energy levels of a coupled system comprising an  $\text{NV}^-$  center and a P1 center. P1 center is a lattice defect in diamond, in which the carbon atom is replaced by a neutral nitrogen atom. P1 center is paramagnetic having the electron spin of 1/2; symmetry properties of this defect center are described by the  $C_{3v}$  group, same as for  $\text{NV}^-$  center. The total number of states in the considered system of two paramagnetic centers (each having a  $^{14}\text{N}$  spin-1 nucleus) is equal to  $54 = 3 \times 3 \times 2 \times 3$ . The interaction between the defect centers is the magnetic dipole-dipole interaction. In the calculation we assume that the symmetry axes of both centers are parallel to the  $\mathbf{B}_0$  vector. Since the energy levels are plotted for the total energy of the system of two defect centers, the energy of the  $M_s = 0$  level of the  $\text{NV}^-$  center is no longer constant, as in Fig. 3(a), but depends on the  $B_0$  field due to the Zeeman interaction of the P1 center with the external field. One can see that in the case under consideration there are multiple level crossings. HFCs and electronic dipole-dipole interaction turn these crossings into LACs. As previously, LACs of the  $M_s = 0$  levels (highlighted with asterisks in the Figure) with the  $M_s = -1$  levels give rise to a decrease of the population of the “bright” state; consequently, sharp LAC lines appear in the spectrum. In the present case, in addition to the lines at around 1024 G more lines appear at around  $B_0 \approx D/2 \approx 500$  G, which are traditionally called “cross-relaxation lines”. Below we demonstrate clearly that these lines are due to the coherent polarization transfer between paramagnetic defect centers.

The analysis of the energy level diagram, like the one shown in Fig. 3, allows one to determine the level crossing points. This is, however, not sufficient for analyzing LAC spectra because one also needs to know the efficiency of polarization transfer between the “bright” and “dark” states at each crossing. Hence, for quantitative analysis of LAC spectra the theoretical treatment needs to be extended.

## B. Simulation method

To calculate LAC spectra, we adapted an approach developed previously to describe coherent polarization transfer in coupled multi-spin systems [45]. In order to use this approach, we also introduce the following sim-

plications:

1. We assume that photo-excitation of the  $\text{NV}^-$  center is a very fast process as compared to the spin dynamics of hyperpolarized  $\text{NV}^-$  centers in the ground state. The same holds for the inter-system crossing processes,  $^3E \rightarrow ^1A_1$  and  $^1E \rightarrow ^3A_2$ , and fluorescence process,  $^3E \rightarrow ^3A_2$ . Hence, we assume that all photo-induced processes do not affect polarization transfer and only provide the initial spin polarization of the  $\text{NV}^-$  center.
2. We consider only the spin evolution of the ground state of the system: the reason is that the system spends only a small fraction of time in the excited state. We also do not see any traces of excited-state LACs in the measured spectrum shown in Fig. 2. We also assume that the spin Hamiltonian of the  $\text{NV}^-$  center interacting with another defect center does not depend on time.
3. We completely neglect spin relaxation. Redistribution of the polarization in the  $\text{NV}^-$  center, as well as between the  $\text{NV}^-$  center and another defect center in the crystal lattice is thus treated as a coherent process in the same manner as before [45, 46].

We introduce the initial spin density matrix of the system in the form of the direct product (Kronecker product) of the individual electronic and nuclear spin density matrices:

$$\rho_0 = \rho_{S1} \otimes \rho_{S2} \otimes \rho_{I1} \otimes \dots \otimes \rho_{In}. \quad (8)$$

Here  $\rho_{S1}$  is the electron spin density matrix of the  $\text{NV}^-$  center is a completely or partially polarized state

$$\rho_{S1} = \alpha \begin{pmatrix} 0 & 0 & 0 \\ 0 & 1 & 0 \\ 0 & 0 & 0 \end{pmatrix} + \frac{1-\alpha}{3} \begin{pmatrix} 1 & 0 & 0 \\ 0 & 1 & 0 \\ 0 & 0 & 1 \end{pmatrix}, \quad (9)$$

where  $\alpha$  is the degree of the light-induced polarization of the  $^3A$  triplet state of the  $\text{NV}^-$  center. The other matrices,  $\rho_{S2}$  (the electron spin density matrix of the second defect center) and  $\rho_{Ii}$  (the nuclear spin density matrices of the  $\text{NV}^-$  center) and  $\rho_{Ij}$  (the nuclear spin density matrices of the second defect center) are the equilibrium density matrices of the corresponding spin systems. Hence, if we neglect the tiny thermal spin polarization, they are equal to  $N^{-1}\hat{E}$  where  $\hat{E}$  is the unity matrix of the corresponding dimensionality  $N$  (here the coefficient  $N^{-1}$  is introduced to provide the normalization condition  $\text{Tr}\{\rho_0\} = 1$ ).

The state described by eq. (8) is a non-stationary state (i.e., it is not an eigen-state) of the Hamiltonian (1); therefore, the density matrix evolves with time. The spin evolution can be described quantitatively in the simplest way in the eigen-basis of the  $\hat{H}$  operator. In this basis, the initial state is as follows:

$$\rho_0^{eb} = \hat{V}^{-1} \rho_0 \hat{V}, \quad (10)$$

where  $\hat{V}$  is the matrix composed of the eigen-vectors of  $\hat{H}$ . Since the Hamiltonian  $\hat{H}$  is time-independent, the matrices  $\hat{V}$  and  $\hat{V}^{-1}$  are the same at any instant of time. In the new basis the Hamiltonian is diagonal and has the following matrix elements:  $\hat{H}_{ij}^{eb} = E_i \delta_{ij}$ , where  $E_i$  is the  $i$ -th eigen-value of the Hamiltonian (i.e., the energy of the  $i$ -th state),  $\delta_{ij}$  is the Kronecker delta. As we express the energy in the frequency units, the density matrix obeys the following equation:

$$i \frac{d\rho_{ij}^{eb}}{dt} = [\hat{H}^{eb}, \rho^{eb}] = 2\pi \sum_k (E_i \delta_{ik} \rho_{kj}^{eb} - \rho_{ik}^{eb} E_k \delta_{kj}) = 2\pi (E_i - E_j) \rho_{ij}^{eb}. \quad (11)$$

Consequently, we can obtain:

$$\rho_{ij}^{eb}(t) = \{\rho_0^{eb}\}_{ij} \exp(-2\pi i \Delta_{ij} t), \quad (12)$$

where  $\Delta_{ij} = E_i - E_j$ .

By going back to the original basis of spin states, we obtain the following expression for the time-dependent density matrix:

$$\rho(t) = \hat{V} \rho^{eb}(t) \hat{V}^{-1}, \quad (13)$$

which allows us to calculate the population of the “bright” state (the  $M_s = 0$  spin state of the  $^3A$  state of the  $\text{NV}^-$  center) at any instant of time:

$$\rho_{00}(t) = \text{Tr}\{\hat{P}_0 \rho(t)\}, \quad (14)$$

where  $\hat{P}_0 = |0\rangle\langle 0|$  is the projector on the  $M_s = 0$  state,  $|0\rangle$ .

The coherent spin evolution described by eq. (14) is interrupted at the instant of time  $t$  after light excitation, i.e., after the  $\text{NV}^-$  center in the ground state absorbs a photon. After that, the system goes back into the initial state, see eq. (8), emitting a photon. If the light intensity is constant, the distribution of the coherent spin evolution times is exponential  $\exp(-t/\tau)/\tau$ , with the mean evolution time,  $\tau$ , depending on the light intensity and the probability of light absorption by the  $\text{NV}^-$  center.

To evaluate the photoluminescence intensity we need to average the  $M_s = 0$  population,  $\rho_{00}(t)$ , over instants of time when the photon is absorbed. This averaged population is as follows:

$$\begin{aligned} \langle \rho_{00} \rangle &= \langle \rho_{00}(t) \rangle = \frac{1}{\tau} \int_0^\infty \rho_{00}(t) \exp(-t/\tau) dt \\ &= \text{Tr}\{\hat{P}_0 \hat{V} \rho^{st} \hat{V}^{-1}\}, \end{aligned} \quad (15)$$

where

$$\begin{aligned} \rho_{ij}^{st} &= \langle \rho^{eb}(t) \rangle_{ij} = \rho_{0,ij}^{eb} \frac{1}{\tau} \int_0^\infty \exp(-t/\tau - 2\pi i \Delta_{ij} t) dt \\ &= \rho_{0,ij}^{eb} / (1 + 2\pi i \Delta_{ij} \tau). \end{aligned} \quad (16)$$

We would like to note that here averaging is performed in the eigen-basis, which makes the calculation much simpler. This is possible because all transformations used here are linear transformations and also due to the fact that the matrices  $\hat{V}$  and  $\hat{V}^{-1}$  are time-independent.

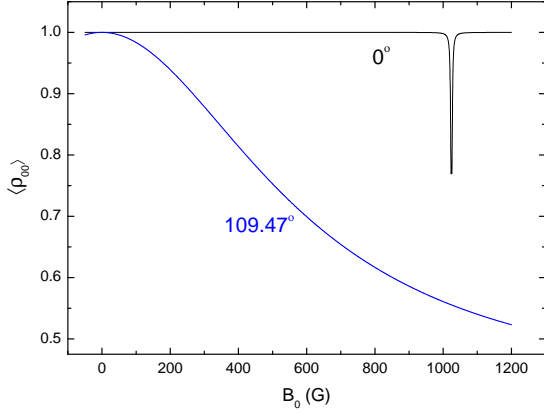


FIG. 4. LAC spectrum of an isolated  $\text{NV}^-$  center for the case  $\mathbf{r}_{\text{NV}} \parallel \mathbf{B}_0$  and for the case where the angle between  $\mathbf{r}_{\text{NV}}$  and  $\mathbf{B}_0$  is equal  $\theta_t$ .

#### IV. RESULTS

##### A. LAC spectra of different systems

In this subsection, we present the calculated LAC spectra for isolated  $\text{NV}^-$  centers as well as for pairs of interacting defect centers. Such calculations allow us to describe different groups of lines found in the experimental LAC spectrum. We would like to emphasize that each calculation can reproduce only some of the observed LAC lines. The reason is that in a real experiment, different  $\text{NV}^-$  centers have different environment. For this reason, the experimental LAC spectrum is a superposition (with appropriate weights) of the spectra for isolated  $\text{NV}^-$  centers as well as for systems comprising an  $\text{NV}^-$  center and another paramagnetic center. In addition, in the proximity of the paramagnetic centers there can also be  $^{13}\text{C}$  nuclei, which affect LACs and become manifest in the observed LAS spectra. Here we present calculations for isolated  $\text{NV}^-$  centers and for  $\text{NV}^-$  centers interacting with other defect centers; such calculations will be done neglecting HFCs to  $^{13}\text{C}$  nuclei and also taking such HFCs into account in order to describe weak satellites to main LAC lines. For the sake of simplicity, in this subsection we always assume a significantly long  $\tau$ ; the effect of the evolution time on the LAC spectra is considered in a separate subsection.

In this work, we always evaluate the photoluminescence signal as the averaged population,  $\langle \rho_{00} \rangle$ , of the  $M_s = 0$  state of the  $\text{NV}^-$ . Hence, we term the  $\langle \rho_{00} \rangle$  dependence on the  $B_0$  magnetic field as “LAC spectrum, assuming that the photoluminescence intensity is directly proportional to  $\rho_{00}$ .”

In Fig. 4 we show the calculated LAC spectrum for a single  $\text{NV}^-$  center. In the calculation we used the Hamiltonian  $\hat{H}$  of the form:

$$\hat{H} = \beta \left[ g_{\parallel} B_{0,z} \hat{S}_z + g_{\perp} (B_{0,x} \hat{S}_x + B_{0,y} \hat{S}_y) \right] +$$

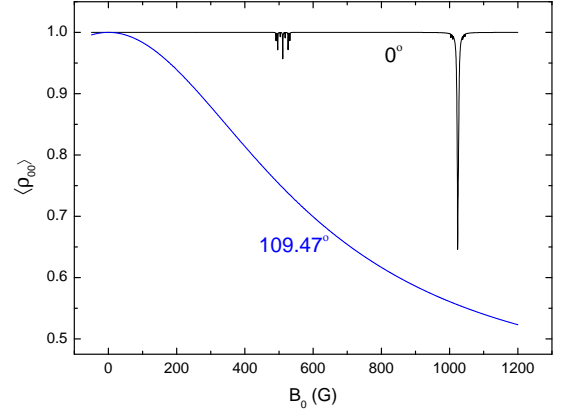


FIG. 5. LAC spectrum of interacting  $\text{NV}^-$  and P1 centers for the orientation where the  $\text{NV}^-$  axis is parallel to the field or tilted by  $\theta_t$ . In the calculation, we have performed averaging over all four possible orientations of the P1 center.

$$+ D \left[ \hat{S}_z^2 - \frac{2}{3} \right] + A_{\parallel} \hat{S}_z \hat{I}_z + A_{\perp} \left[ \hat{S}_x \hat{I}_x + \hat{S}_y \hat{I}_y \right] + P \left[ \hat{I}_z^2 - \frac{1}{3} I(I+1) \right]. \quad (17)$$

Hereafter, in calculations we use the following magnetic parameters for the  $\text{NV}^-$  center [47]:  $g_{\parallel} = 2.0029$ ,  $g_{\perp} = 2.0031$ ,  $D_1 = 2872$  MHz,  $E = 0$ ,  $A_{\parallel} = -2.2$  MHz,  $A_{\perp} = -2.7$  MHz,  $Q = -4.8$  MHz.

When the symmetry axis of the  $\text{NV}^-$  center is parallel to external field vector  $\mathbf{B}_0$ , there is a single sharp LAC line at the field of 1024 G, where the  $M_s = 0$  and  $M_s = -1$  levels cross, as shown in Fig.3. At this LAC, the HFC to the  $^{14}\text{N}$  nucleus of the defect center becomes active, turning the level crossing into a LAC. Due to spin mixing at this LAC, the population of the “bright” state is reduced and a dip in the luminescence intensity is found. When the angle between the  $\mathbf{r}_{\text{NV}}$  and  $\mathbf{B}_0$  vectors is equal to  $\theta_t$  there are no level crossings (see Fig.3); consequently, there are no sharp lines in the spectrum. Instead, there is a smooth decay of the population of the  $M_s = 0$  state upon increase of the field strength. A similar decrease of the photoluminescence can be observed experimentally, as can be seen in Fig.2. The reason for this effect is that the field component, which is perpendicular to the  $\text{NV}^-$  symmetry axis, gives rise to transitions between the triplet sublevels of the ground state. As a result, the “bright”  $M_s = 0$  state is mixed with the “dark”  $M_s = \pm 1$  states and its population decreases giving rise to the decrease of the photoluminescence intensity. Hence, the calculation for an isolated  $\text{NV}^-$  center can describe the smooth decay of the luminescence intensity with increasing magnetic field strength and also the LAC line at 1024 G but not other LAC lines found in experiments. To describe these lines, we need to perform calculations for two interacting defect centers with one of them being the  $\text{NV}^-$  center.

In Fig. 5 we show the calculated LAC spectrum for the system of two interacting defect centers,  $\text{NV}^-$  center



and P1 center. In the calculation, we make use of the Hamiltonian given by eqs. (1-3), where  $S_1$ ,  $I_1$ ,  $\mathcal{G}_1$ ,  $\mathcal{A}_1$ ,  $\mathcal{Q}_1$  being the parameters of the  $\text{NV}^-$  center, whereas  $S_2$ ,  $I_2$ ,  $\mathcal{G}_2$ ,  $\mathcal{A}_2$ ,  $\mathcal{Q}_2$  are the parameters of the P1 center. In the calculation, we use the following parameters:  $g_{||}^2 = g_{\perp}^2 = 2.0023$ ,  $A_{||}^2 = 114$  MHz,  $A_{\perp}^2 = 81$  MHz,  $Q_2 = Q_1 = -4.8$  MHz,  $D_{dd} = 1$  MHz. Hence, the parameters for the  $\text{NV}^-$  center are the same as those in the calculation shown in Fig. 4. All calculations are performed using averaging over the four possible orientations of the P1 center.

When the angle between the  $\mathbf{B}_0$  and  $\mathbf{r}_{\text{NV}}$  vectors is equal to  $\theta_t$ , like in the previous case, there is a smooth decrease of  $\langle \rho_{00} \rangle$  upon increasing the magnetic field strength and no sharp lines are seen. The reason for this is exactly the same as in the previous case of an isolated  $\text{NV}^-$  center: there is mixing of the triplet sublevels by the perpendicular field component and there are no level crossings.

In the case  $\mathbf{r}_{\text{NV}} \parallel \mathbf{B}_0$ , in the LAC spectrum there are two groups of sharp lines seen at around 1024 G and at around 500 G. These lines are also discussed below in further detail. They are caused by the level crossings shown in Fig. 3; however, we would like to stress that in the calculation presented in Fig. 5 all four possible orientations of the P1 center are taken into account. The fact that the two groups of lines are found at the magnetic fields of about  $D_1$  and  $D_1/2$  is due to the very small difference in the  $g$ -factors of the  $\text{NV}^-$  center and P1 center. Hence, the present calculation can account for the LAC lines at around 500 G.

In Fig. 6 we show the calculation result for a pair of  $\text{NV}^-$  centers, where one of them is oriented parallel to  $\mathbf{B}_0$ , while the other one is oriented at the  $\theta_t$  angle to the magnetic field. In the calculation, averaging over three possible orientation of the second  $\text{NV}^-$  center is performed. Parameters of the calculation are the same as those in previous calculations. For calculating the LAC spectra, we use different degree of spin polarization  $\alpha$  of the  $\text{NV}^-$  centers having different orientations with respect to the magnetic field. The reason is that the probability of absorbing a photon by an  $\text{NV}^-$  center depends on the polarization of the incident light. Specifically, the absorption probability is maximal when the polarization vector is perpendicular to  $\mathbf{r}_{\text{NV}}$  being close to zero when the two vectors are parallel. In our experiments, the polarization vector is always perpendicular to the external magnetic field. Therefore, we always assume that when  $\mathbf{r}_{\text{NV}}$  is parallel to  $\mathbf{B}_0$  then  $\alpha \rightarrow 1$  (maximal spin polarization), while for the other orientations we take  $\alpha = 0.7$ .

When the angle between the  $\mathbf{r}_{\text{NV}}$  and  $\mathbf{B}_0$  vectors is equal to  $\theta_t$ , like in the previous case (and for the same reason), there is a smooth decrease of  $\langle \rho_{00} \rangle$  with the field. Besides this, at any orientation of the  $\text{NV}^-$  center there are three sharp LAC lines at zero field, at 590 G and at 1024 G. The lines at zero field and at 590 G have different signs for the different orientations of the  $\text{NV}^-$  center. It is worth noting, that the zero-field line has exactly the

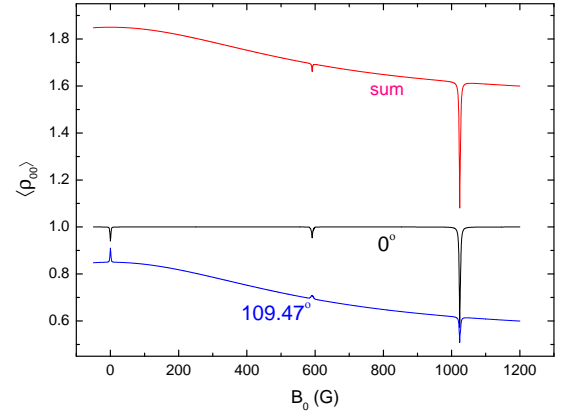


FIG. 6. LAC spectrum of a system of two interacting  $\text{NV}^-$  centers; one of them is oriented parallel to the magnetic field and the other one is oriented at the  $\theta_t$  angle to the field (averaging over the three possible orientations of the second center is performed). The degree of polarization  $\alpha$  (see eq. (9)) for the first  $\text{NV}^-$  center is equal to 1; for the second center it is 0.7. In the plot we show the average population  $\langle \rho_{00} \rangle$  of the  $M_s = 0$  state for each  $\text{NV}^-$  center as well as the sum of these populations.

same amplitude for the different orientations considered here; consequently, the total polarization does not have a feature at zero field. This is consistent with the assumption [28] that this line is merely due to the polarization transfer between  $\text{NV}^-$  centers with different orientations. In experiments this line becomes visible only because the luminescence intensity of the differently oriented  $\text{NV}^-$  centers is not the same (due to the different absorption efficiency of the incident light). As a consequence, the zero-field LAC line (in contrast to all other LAC lines) is a second-order effect and its intensity quadratically depends on the light intensity [28].

Hence, our calculation can account for additional LAC lines at around 500 G and 590 G, which were reported before and come from polarization exchange between different defect centers. In the literature these lines are usually named “cross-relaxation lines” as they are associated with polarization transfer. We would like to stress that such a term is, perhaps, misleading because in magnetic resonance cross-relaxation usually means polarization transfer mediated by stochastic, not dynamics, processes [48, 49]. In the present case the “cross-relaxation lines” obviously originate from coherent exchange of polarization at corresponding LACs.

## B. Comparison with experiment

Having understood the nature of different lines in LAC spectra, we can compare our theoretical considerations with the experimental results and analyze the origin of different lines (or groups of lines) found experimentally.

The experimental LAC spectra in their original ap-

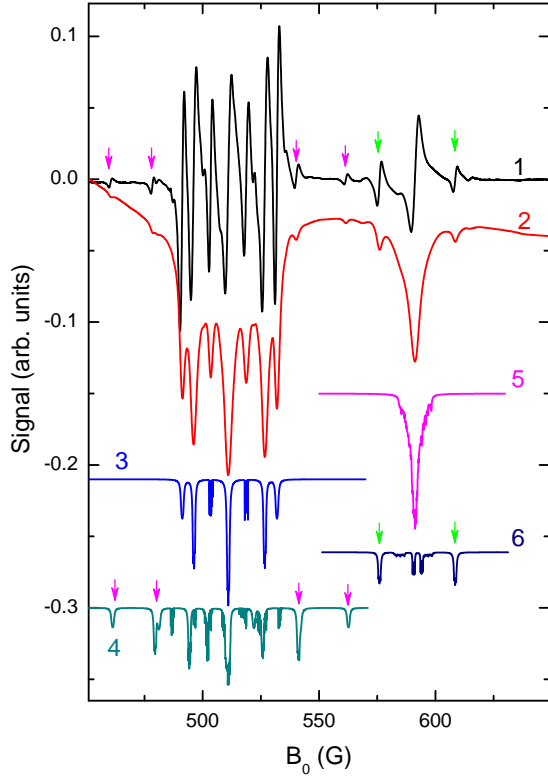


FIG. 7. Experimental LAC spectrum in the field range 450-650 G (curve 1) and integrated spectrum (curve 2). Curves 3-6 present the calculated LAC spectrum for the pair  $\text{NV}^-/\text{P1}$  (curve 3); for the pair  $\text{NV}^-/\text{P1}$  assuming that the P1 center has a  $^{13}\text{C}$  nucleus at the  $\text{C}_1$  position (curve 4); for the pair  $\text{NV}^-/\text{NV}^-$  with different orientations taking into account a  $^{13}\text{C}$  spin in the proximity of one of the two centers (curve 5); for the pair  $\text{NV}^-/\text{NV}^-$  when one of the centers has a  $^{13}\text{C}$  nucleus (curve 6). Arrows indicate the lines in the LAC spectrum, which become manifest due to the HFC with  $^{13}\text{C}$  nuclei.

pearance and also integrated spectra in the field range 450-650 G are shown in Fig. 7. Additionally, in this figure we present the calculation results for different pairs of interacting paramagnetic centers. All parameters of  $\text{NV}^-$  centers and P1 centers are the same as those given above. In the calculation, the first center is always an  $\text{NV}^-$  center oriented parallel to the  $\mathbf{B}_0$  center; we perform averaging over all four possible orientations of the P1 center (single orientation parallel to the field and three orientations where the P1 centers are tilted by  $\theta_t$ ) and for all three possible orientations of the second  $\text{NV}^-$  center (where the angle between  $\mathbf{B}_0$  and  $\mathbf{r}_{\text{NV}}$  is equal to  $\theta_t$ ).

One can see that the calculation performed for the  $\text{NV}^-/\text{P1}$  pair very well describes the seven previously reported LAC lines in the range 490-540 G. We would like to stress that our model can describe not only the positions of the lines, but also their relative amplitudes. The calculation run for the  $\text{NV}^-/\text{NV}^-$  pair also very well reproduces the line at 590 G.

For assigning other lines, namely, the weak satellite lines indicated in Fig. 7 we performed a calculation assuming that the defect centers have the HFC with sur-

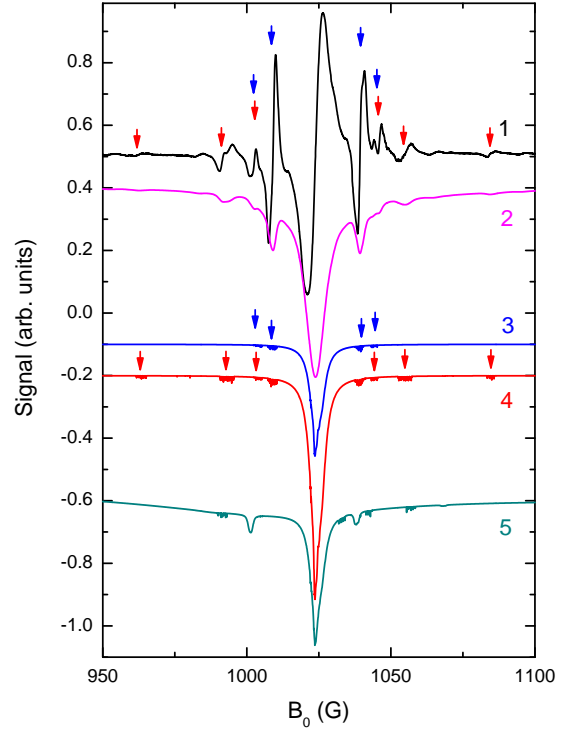


FIG. 8. Experimental LAC spectrum in the range 950-1100 G (curve 1) and integrated spectrum (curve 2). Calculation for pairs of interacting defect centers: pair  $\text{NV}^-/\text{P1}$  (curve 3); pair  $\text{NV}^-/\text{P1}$  taking into account coupling of the P1 center to a  $^{13}\text{C}$  spin in the  $\text{C}_1$  position (curve 4); pair  $\text{NV}^-/\text{NV}^-$  with different orientations taking into account a  $^{13}\text{C}$  spin in the proximity of one of the two centers (curve 5). Arrows indicate the corresponding lines in the experimental and calculated LAC spectra.

rounding carbon nuclei in the lattice. In the sample studied,  $^{13}\text{C}$  nuclei are present at the low natural abundance of 1.1%. For this reason, we also perform simulations taking into account the fact that one of the two centers has a  $^{13}\text{C}$  spin in the close proximity to the paramagnetic defect. For this carbon nucleus in the  $\text{C}_1$  position we use the following HFC parameters: for the  $\text{NV}^-$  center  $A_{||} = A_{\perp} = 100$  MHz, for the P1 center  $A_{||} = 340$  MHz,  $A_{\perp} = 140$  MHz [50].

The LAC spectra calculated taking into account the additional HFC terms are also presented in Fig. 7. In the figure, the arrows indicate the weak satellite lines in the experimental spectrum and also in the simulated spectra. One can readily see that there is a very good agreement between the positions of the lines in the experimental and calculated spectra. As far as the amplitude of these lines is concerned, the relative intensities of the lines caused by the additional HFC in the P1 center are reproduced properly. Additionally, the calculation can describe the doublet seen in the spectrum at 477 G.

However, if we keep in mind the low natural abundance of  $^{13}\text{C}$  nuclei in the sample, the amplitude of the satellite lines in the calculation is much smaller than that found



experimentally. This is true for the pair  $NV^-/P1$  and even to a greater extent for the pair  $NV^-/NV^-$ . Most likely, this discrepancy is caused by the effect of field modulation on LAC lines [34]: at low frequencies the line amplitude strongly increases, this effect is much more pronounced for weak low-amplitude lines.

One more group of LAC lines is found at around 1024 G; close inspection shows that in addition to the main line there are also weak satellite lines seen in the spectrum. In Fig. 8 we show the LAC spectrum in its original appearance together with the calculated spectra for different pairs of interacting defect centers: pair  $NV^-/P1$  and also pairs  $NV^-/P1$  and  $NV^-/NV^-$  hyperfine-coupled to nearest  $^{13}C$  nuclei. In the case of the  $NV^-/P1$  pair we take into account the coupling to a  $^{13}C$  nucleus in the  $C_1$  position in the P1 center. All calculation parameters are the same as those in previous calculations.

The LAC lines in the spectra calculated for different pairs strongly overlap, therefore it is problematic to assign specific lines. We can state only that the weak lines at the wings of the spectrum shown in Fig. 8 are caused by the HFC to a  $^{13}C$  nucleus in the P1 center. From the calculation, we can also deduce that some asymmetry of the spectrum is caused by the HFCs to carbon nuclei in the  $NV^-/NV^-$  pair. As far as relative amplitude of individual lines are concerned, the amplitude of the satellite lines is much stronger in experiments than in the calculation; this effect is even more pronounced as compared to the spectra shown in Fig. 7.

### C. Effect of the average evolution time $\tau$

Appearance of LAC spectra also depends on the evolution time  $\tau$  because spin mixing at each LAC requires finite time to develop. Specifically, when the minimal splitting at a LAC is equal to  $2|V_{\mu\nu}| \neq 0$  the characteristic mixing time is of the order of  $1/|V_{\mu\nu}|$ . When this time is much longer than  $\tau$  the corresponding LAC would not reveal itself as a feature in the magnetic field dependence of photoluminescence. Hence, to observe a feature coming from a LAC the evolution time should be greater than or comparable to  $1/|V_{\mu\nu}| \neq 0$ ;  $\tau \approx 1/|V_{\mu\nu}| \neq 0$  gives a threshold value for observing the feature.

In our calculation method, the evolution time  $\tau$  is an input parameter, which is difficult to estimate. For this reason, we need to know how critical is the  $\tau$  dependence of LAC line intensities. In Figs. 9, 10 we present the LAC spectra calculated for different  $\tau$  values considering a pair of defects coupled by dipole-dipole interaction of the strength of 1 MHz. The parameter  $\tau$  is varied over a wide range from  $10^{-8}$  to  $10^{-1}$  s. One can readily see that there is a certain threshold  $\tau$  value: above this value the spectrum almost does not change. For the LAC line at 1024 G this value is approximately  $10^{-7}$  s (see Fig. 9). The weak satellite lines are more sensitive to the  $\tau$  value, as can be seen from Fig. 10. For these lines, the threshold

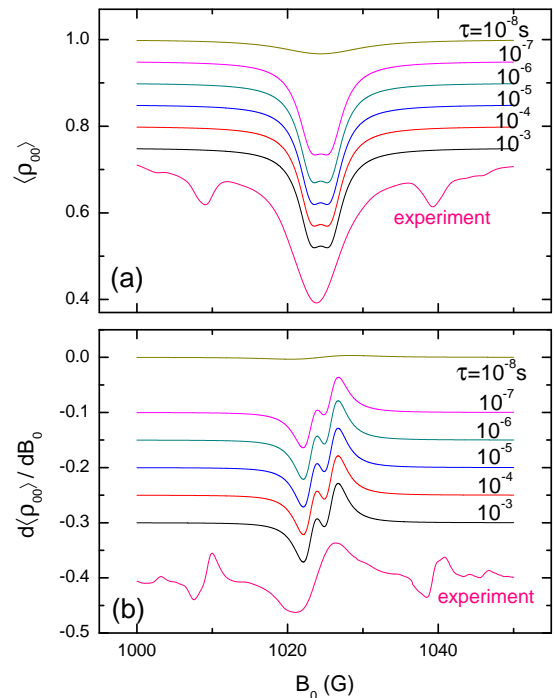


FIG. 9. Dependence of the LAC spectrum (shown in the range around 1024 G) on the mean evolution time  $\tau$  for an isolated  $NV^-$  center. We present the calculated  $\langle \rho_{00} \rangle$  field dependence and the integrated experimental LAC spectrum (subplot a) and also the  $B_0$  derivative of  $\langle \rho_{00} \rangle$  and the experimental spectrum in its original appearance (subplot b).

$\tau$  value is about  $10^{-5}$  s. In all calculations, we use the value  $\tau = 10^{-4}$  s, which guarantees correct evaluation of the spectra in all cases (meaning that all LAC lines of interest become manifest).

The theoretical curves in Fig. 9 exhibit a splitting of the main LAC line at 1024 G. In experiments such an effect is not observed, which we attribute to a relatively high amplitude of field modulation, which is 0.5 G, lowering the resolution. From comparison of Figs. 9 and 10 we can draw one more conclusion: in Fig. 9 the position of the LAC line of an isolated  $NV^-$  center is shifted to higher fields as compared to the experimental observation (by approximately 0.5 G). For the  $NV^-/P1$  pair, this line is slightly distorted (see Fig. 10) so that the low-field component becomes stronger and the high-field component becomes weaker. As a result, there is only one LAC line present in the spectrum and its position precisely fits to that found experimentally. Hence, we can conclude that the pair  $NV^-/P1$  makes the dominant contribution to the line at 1024 G.

## V. DISCUSSION

Hence, we present a method, which can be used to treat quantitatively LAC spectra in diamond crystals contain-

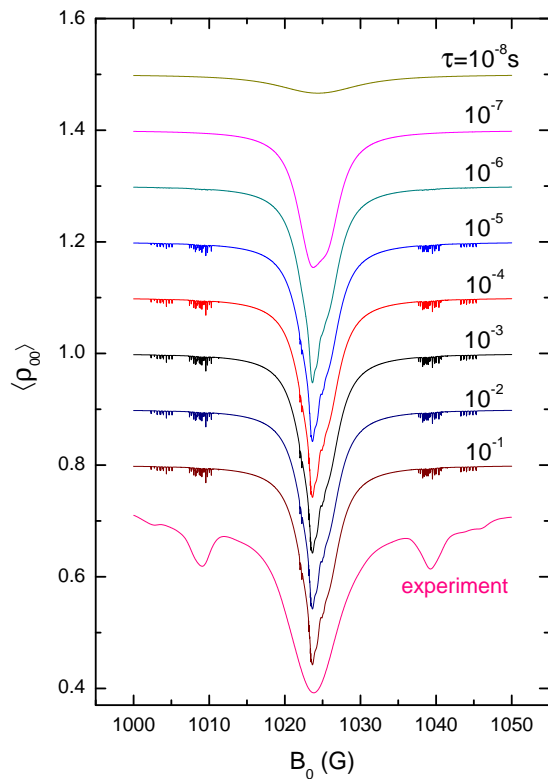


FIG. 10. Dependence of the LAC spectrum for the pair  $\text{NV}^-/\text{P1}$  of interacting defect centers on the mean evolution time  $\tau$  and the experimental LAC spectrum (here the integrated spectrum is presented).

ing paramagnetic color centers. The method uses only standard linear algebra methods, such as matrix multiplication and solution of the eigen-problem of a hermitian matrix. Consequently, we are able to treat multi-spin systems that are described by Hamiltonians of a large dimensionality. For instance, here we consider the system of four spins 1 (two spin-1 paramagnetic defects each having a spin-1  $^{14}\text{N}$  nucleus) and one spin-1/2  $^{13}\text{C}$  nucleus; in this case the Hamiltonian is a  $162 \times 162$  matrix. Our approach can be easily extended to systems containing color centers other than  $\text{NV}^-$  centers. The main simplifying assumption used here is neglecting the spin evolution in the excited state: when necessary, the spin evolution in the excited state can be treated by using the same method by redefining the time  $\tau$  as the lifetime of the excited state. A more rigorous approach, which would explicitly take into account the evolution in both states and transitions between them can also be implemented, see e.g. Ref. [43], but it is significantly more time consuming.

Our treatment shows that the positions of LAC lines can be accurately described by the proposed theoretical approach. We would like to note that the calculations shown here do not use any free parameters other than the evolution time (which does not strongly affect LAC spectra): the parameters of the relevant interaction ten-

sors are taken from independent measurements reported in literature. As far as the relative amplitudes of LAC lines are concerned, our method precisely describes the amplitudes of lines belonging to the same group. This is true, for instance, for the lines found in the range 490-540 G, which are conditioned by coupling of the electron spins of  $\text{NV}^-$  centers and P1 centers. The same situation holds for the lines found in the range 450-650 G: these lines are due to  $^{13}\text{C}$  nuclei in the  $\text{C}_1$  position of the P1 center. However, the satellite lines at around 1024 G, as well as the satellite lines in the range 450-650 G, which are due to HFC to  $^{13}\text{C}$  nuclei (present only in low concentration), in experiments are much stronger than expected from the theoretical treatment.

Field modulation effects are not included in our simulations (this is not feasible with available computational resources) but on the qualitative level the influence of modulation can be rationalized from our previous work [34]. Specifically, we have considered the effect of field modulation on the amplitude of LAC lines and demonstrated that the line amplitudes strongly increase at low modulation frequencies. Furthermore, for weak lines such an increase is associated with polarization transfer to nuclear spins giving rise to an even stronger increase of the line amplitude. Specifically, for weak LAC lines the increase in amplitude upon decreasing the modulation frequency from 12.5 kHz to 17 Hz is an order of magnitude stronger than for intense lines, e.g., than for the LAC line at 1024 G. Thus, the amplitude ratio calculated by using our method is more similar to experimental observations at the modulation frequency of 12.5 kHz, rather than to those at 17 Hz. Numerical calculations [34] show that such an enhancement of LAC lines is due to the fact that nuclear spins, which relax much slower than the electron spins, can store spin polarization. After many excitation-radiation cycles (or excitation-radiationless relaxation), the polarization is transferred from  $\text{NV}^-$  centers to nuclei. Due to the much slower spin relaxation, nuclei can store polarization; subsequently, polarization transfer back to  $\text{NV}^-$  can occur. Such polarization transfer is most efficient at low modulation frequencies; in the present theoretical model it is not taken into account.

## VI. CONCLUSIONS

We propose a numerically efficient method for describing LAC spectra of  $\text{NV}^-$  centers in diamond crystals. From the mathematical viewpoint, the method makes use of the solution of the eigen-problem of hermitian matrices and basic matrix operators. Standard numerical algorithms for such calculations are well established and efficient, allowing one to implement the proposed method. The method allows one to predict not only the positions of LAC lines, but also their shapes and relative intensities; hence, we are able to model the main groups of lines in LAC spectra, assign lines to specific LACs and analyze satellites coming from  $^{13}\text{C}$  nuclei at low natural

abundance. We expect that the proposed method can be used to determine magnetic resonance parameters of dark defect centers interacting with  $NV^-$  centers and also to investigate such interactions.

## ACKNOWLEDGMENTS

The work was supported by the Russian Foundation for Basic Research (Grant No. 16-03-00672 and 17-03-00932).

- 
- [1] M. W. Doherty, N. B. Manson, P. Delaney, F. Jelezko, J. Wrachtrup, and L. C. L. Hollenberg, *Phys. Reports* **528**, 1 (2013).
  - [2] G. Balasubramanian, I. Y. Chan, R. Kolesov, M. Al-Hmoud, J. Tisler, C. Shin, C. Kim, A. Wojcik, P. R. Hemmer, A. Krueger, T. Hanke, A. Leitenstorfer, R. Bratschitsch, F. Jelezko, and J. Wrachtrup, *Nature (London)* **455**, 648 (2008).
  - [3] L. Rondin, J.-P. Tetienne, T. Hingant, J.-F. Roch, P. Maletinsky, and V. Jacques, *Rep. Prog. Phys.* **77**, 056503 (2014).
  - [4] R. Schirhagl, K. Chang, M. Loretz, and C. L. Degen, *Annu. Rev. Phys. Chem.* **65**, 83 (2014).
  - [5] G. Kucsko, P. C. Maurer, N. Y. Yao, M. Kubo, H. J. Noh, P. K. Lo, H. Park, and M. D. Lukin, *Nature (London)* **500**, 54 (2013).
  - [6] P. Neumann, I. Jakobi, F. Dolde, C. Burk, R. Reuter, G. Waldherr, J. Honert, T. Wolf, A. Brunner, J. H. Shim, D. Suter, H. Sumiya, J. Isoya, and J. Wrachtrup, *Nano Lett.* **13**, 2738 (2013).
  - [7] F. Jelezko, T. Gaebel, I. Popa, M. Domhan, A. Gruber, and J. Wrachtrup, *Phys. Rev. Lett.* **93**, 130501 (2004).
  - [8] P. C. Maurer, G. Kucsko, C. Latta, L. Jiang, N. Y. Yao, S. D. Bennett, F. Pastawski, D. Hunger, N. Chisholm, M. Markham, D. J. Twitchen, J. I. Cirac, and M. D. Lukin, *Science* **336**, 1283 (2012).
  - [9] T. van der Sar, Z. H. Wang, M. S. Blok, H. Bernien, T. H. Taminiau, D. M. Toyli, D. A. Lidar, D. D. Awschalom, R. Hanson, and V. V. Dobrovitski, *Nature (London)* **484**, 82 (2012).
  - [10] F. Dolde, I. Jakobi, B. Naydenov, N. Zhao, S. Pezzagna, C. Trautmann, J. Meijer, P. Neumann, F. Jelezko, and J. Wrachtrup, *Nat. Phys.* **9**, 139 (2013).
  - [11] F. Dolde, V. Bergholm, Y. Wang, I. Jakobi, B. Naydenov, S. Pezzagna, J. Meijer, F. Jelezko, P. Neumann, T. Schulte-Herbrüggen, B. Jacob, and J. Wrachtrup, *Nature Communications* **5**, 3371 (2014).
  - [12] L. T. Hall, G. C. G. Beart, E. A. Thomas, D. A. Simpson, L. P. McGuinness, J. H. Cole, J. H. Manton, R. E. Scholten, F. Jelezko, J. Wrachtrup, S. Petrou, and L. C. L. Hollenberg, *Sci. Rep.* **2**, 401 (2012).
  - [13] J. F. Barry, M. J. Turner, J. M. Schloss, D. R. Glenn, Y. Song, M. D. Lukin, H. Park, and R. L. Walsworth, *Proc. Natl. Acad. Sci. (U.S.A.)* **113**, 14133 (2016).
  - [14] S. Steinert, F. Ziem, L. T. Hall, A. Zappe, M. Schweikert, N. Götz, A. Aird, G. Balasubramanian, L. Hollenberg, and J. Wrachtrup, *Nat. Commun.* **4**, 1607 (2013).
  - [15] I. Lovchinsky, A. O. Sushkov, E. Urbach, N. P. de Leon, S. Choi, K. D. Greve, R. Evans, R. Gertner, E. Bersin, C. Müller, L. McGuinness, F. Jelezko, R. L. Walsworth, H. Park, and M. D. Lukin, *Science* **351**, 836 (2016).
  - [16] A. Gruber, A. Dräbenstedt, C. Tietz, L. Fleury, J. Wrachtrup, and C. von Borczyskowski, *Science* **276**, 1212 (1997).
  - [17] D. Suter and F. Jelezko, *Prog. Nucl. Magn. Reson. Spectrosc.* **98-99**, 50 (2017).
  - [18] G. Balasubramanian, P. Neumann, D. Twitchen, M. Markham, R. Kolesov, N. Mizuochi, J. Isoya, J. Achard, J. Beck, J. Tissler, V. Jacques, P. R. Hemmer, F. Jelezko, and J. Wrachtrup, *Nature Materials* **8**, 383 (2009).
  - [19] M. V. Gurudev Dutt, L. Childress, L. Jiang, E. Togan, J. Maze, F. Jelezko, A. S. Zibrov, P. R. Hemmer, and M. D. Lukin, *Science* **316**, 1312 (2007).
  - [20] P. Neumann, N. Mizuochi, F. Rempp, P. Hemmer, H. Watanabe, S. Yamasaki, V. Jacques, T. Gaebel, F. Jelezko, and J. Wrachtrup, *Science* **320**, 1326 (2008).
  - [21] R. Hanson, F. M. Mendoza, R. J. Epstein, and D. D. Awschalom, *Phys. Rev. Lett.* **97**, 087601 (2006).
  - [22] E. van Oort and M. Glasbeek, *Phys. Rev. B* **40**, 6509 (1989).
  - [23] R. J. Epstein, F. M. Mendoza, Y. K. Kato, and D. D. Awschalom, *Nat. Phys.* **1**, 94 (2005).
  - [24] L. J. Rogers, S. Armstrong, M. J. Sellars, and N. B. Manson, *New J. Phys.* **10**, 103024 (2008).
  - [25] L. J. Rogers, R. L. McMurtrie, M. J. Sellars, and N. B. Manson, *New J. Phys.* **11**, 063007 (2009).
  - [26] N. Lai, D. Zheng, F. Jelezko, F. Treussart, and J.-F. Roch, *Appl. Phys. Lett.* **95**, 133101 (2009).
  - [27] S. Armstrong, L. J. Rogers, R. L. McMurtrie, and N. B. Manson, *Physics Procedia* **3**, 1569 (2010).
  - [28] S. V. Anishchik, V. G. Vins, A. P. Yelissev, N. N. Lukzen, N. L. Lavrik, and V. A. Bagryansky, *New J. Phys.* **17**, 023040 (2015).
  - [29] D. A. Broadway, J. D. A. Wood, L. T. Hall, A. Stacey, M. Markham, D. A. Simpson, J.-P. Tetienne, and L. C. L. Hollenberg, *Phys. Rev. Applied* **6**, 064001 (2016).
  - [30] L. T. Hall, P. Kehayias, D. A. Simpson, A. Jarmola, A. Stacey, D. Budker, and L. C. L. Hollenberg, *Nature Communications* **7**, 10211 (2016).
  - [31] A. Wickenbrock, H. Zheng, L. Bougas, N. Leefer, S. Afach, A. Jarmola, V. M. Acosta, and D. Budker, *Appl. Phys. Lett.* **109**, 053505 (2016).
  - [32] A. N. Anisimov, R. A. Babunts, S. V. Kidalov, E. N. Mokhov, V. A. Soltamov, and P. G. Baranov, *JETP Letters* **104**, 82 (2016).
  - [33] H. Zheng, G. Chatzidrosos, A. Wickenbrock, L. Bougas, R. Lazda, A. Berzins, F. H. Gahbauer, M. Auzinsh, R. Ferbers, and D. Budker, *Proc. SPIE* **10119**, 101190X (2017).
  - [34] S. V. Anishchik and K. L. Ivanov, *Phys. Rev. B* **96**, 115142 (2017).
  - [35] R. Akhmedzhanov, L. Gushchin, N. Nizov, V. Nizov, D. Sobgayda, and I. Zelensky, *Phys. Rev. A* **96**, 013806 (2017).
  - [36] P. Delaney, J. C. Greer, and J. A. Larsson, *Nano Lett.* **10**, 610 (2010).

- [37] L. Robledo, H. , Bernien, T. van der Sar, and R. Hanson, *New J. Phys.* **13**, 025013 (2011).
- [38] M. L. Goldman, M. W. Doherty, A. Sipahigil, N. Y. Yao, S. D. Bennett, N. B. Manson, A. Kubanek, and M. D. Lukin, *Phys. Rev. B* **91**, 165201 (2015).
- [39] G. Thiering and A. Gali, *Phys Rev B* **98**, 085207 (2018).
- [40] J. H. N. Loubser and J. A. Van Wyk, *Diamond Research* **1**, 11 (1977).
- [41] N. B. Manson, J. P. Harrison, and M. J. Sellars, *Phys. Rev. B* **74**, 104303 (2006).
- [42] V. Ivády, K. Szász, A. L. Falk, P. V. Klimov, D. J. Christle, E. Janzén, I. A. Abrikosov, D. D. Awschalom, and A. Gali, *Phys. Rev. B* **92**, 115206 (2015).
- [43] D. V. Sosnovsky and K. L. Ivanov, *Mol. Phys.* (2018), DOI: 10.1080/00268976.2018.1504996.
- [44] M. Mehring, *High Resolution NMR Spectroscopy in Solids*, edited by P. Diehl, E. Fluck, and R. Kosfeld, NMR Basic Principles and Progress, Vol. 11 (Springer-Verlag, Berlin-Heidelberg-New York, 1976).
- [45] K. L. Ivanov, A. V. Yurkovskaya, and H.-M. Vieth, *J. Chem. Phys.* **129**, 234513 (2008).
- [46] K. L. Ivanov, K. Miesel, A. V. Yurkovskaya, S. E. Korchak, A. S. Kiryutin, and H.-M. Vieth, *Appl. Magn. Reson.* **30**, 513 (2006).
- [47] B. V. Yavkin, G. V. Mamin, and S. B. Orlinskii, *J. Magn. Res.* **262**, 15 (2016).
- [48] I. Solomon, *Phys. Rev.* **99**, 559 (1955).
- [49] W. A. Anderson and R. Freeman, *J. Chem. Phys.* **37**, 85 (1962).
- [50] A. G. Every and D. S. Schonland, *Solid State Commun* **3**, 205 (1965).